

# Density functional theory of fluids in the isothermal-isobaric ensemble

A. González, J. A. White, F. L. Román, and S. Velasco

*Departamento de Física Aplicada, Universidad de Salamanca. E-37008 Salamanca, Spain*

(Received 23 February 2004; accepted 19 March 2004)

We present a density functional theory for inhomogeneous fluids at constant external pressure. The theory is formulated for a volume-dependent density,  $n(\mathbf{r}, V)$ , defined as the conjugate variable of a generalized external potential,  $\nu(\mathbf{r}, V)$ , that conveys the information on the pressure. An exact expression for the isothermal-isobaric free-energy density functional is obtained in terms of the corresponding canonical ensemble functional. As an application we consider a hard-sphere system in a spherical pore with fluctuating radius. In general we obtain very good agreement with simulation. However, in some situations a peak develops in the center of the cavity and the agreement between theory and simulation becomes worse. This happens for systems where the number of particles is close to the *magic* numbers  $N=13, 55$ , and  $147$ . © 2004 American Institute of Physics. [DOI: 10.1063/1.1739395]

## I. INTRODUCTION

Understanding the properties of small systems has become a subject of fundamental importance for physics and chemistry due to the rapid development of the science and technology of nanomaterials. A key issue in the theoretical and simulation study of small systems is the well-known fact that the various statistical mechanics ensembles are not equivalent as it happens in the thermodynamic limit.<sup>1</sup> This implies that one must carefully determine the influence of the surroundings in order to choose the most appropriate ensemble for the study of the system. The isothermal-isobaric ensemble<sup>1</sup> has been widely used in Monte Carlo (MC) simulation<sup>2</sup> of a large variety of systems since in many experimental situations one is working with a fixed number of particles at constant external pressure and temperature. Also, this is the natural ensemble for the study of phase transitions.<sup>2</sup> From a theoretical viewpoint it has been suggested very recently that, as happens for the uniform fluid of hard-rods,<sup>3</sup> an isothermal-isobaric approach could be of relevance in the study of one-dimensional inhomogeneous systems with arbitrary interactions,<sup>4</sup> and single-file, cylindrically bounded fluids.<sup>5</sup>

In this work we present a density functional theory (DFT) approach that is shown to be of practical application in the study of inhomogeneous systems in the isothermal-isobaric ensemble. As an example we consider a small system of hard spheres confined to a hard spherical cavity with fluctuating volume. We also present MC simulations of the system in order to test the theory. The paper is structured as follows. Using results for the canonical ensemble, the isothermal-isobaric theory is developed in Sec. II. An exact expression for the free-energy functional in the isothermal-isobaric ensemble is derived in terms of its canonical ensemble counterpart. The Euler–Lagrange equation for this functional allows us to obtain the isothermal-isobaric equilibrium density as a weighted average of canonical ensemble densities. In Sec. III the results of the DFT approach are compared with MC data. This comparison shows that, in

some situations, important differences arise between theory and simulation for the density profile in the center of the spherical cavity. A detailed study of these situations is presented in Sec. IV, where we analyze the dependence of the profile with the number of particles and the external pressure of the system. We conclude with a brief summary of the main results of the paper.

## II. THEORY

The isothermal-isobaric partition function  $\Delta_N$  of a fluid composed by  $N$  particles at temperature  $T$  and external pressure  $P$  can be expressed as

$$\Delta_N = \int_0^\infty \exp(-\beta PV) Q_{N,V}[V_{\text{ext}}] \frac{dV}{\delta_V}, \quad (1)$$

where  $\beta=1/k_B T$  is the inverse temperature and the volume scale  $\delta_V$  is included to ensure that  $\Delta_N$  is a dimensionless quantity.  $Q_{N,V}[V_{\text{ext}}]$  denotes the canonical partition function which, for fixed intermolecular potential, is a functional of the external potential  $V_{\text{ext}}$ . Equation (1) can be rewritten as

$$\Delta_N = \int_0^\infty Q_{N,V}[\nu] \frac{dV}{\delta_V}, \quad (2)$$

where  $\nu(\mathbf{r}, V) \equiv V_{\text{ext}}(\mathbf{r}, V) + PV/N$  is a generalized external potential in which  $V_{\text{ext}}$  may also depend on the volume  $V$ . We note that the definition of  $\nu$  could be extended by considering the fluctuating volume ensemble suggested by Attard and Moule<sup>6</sup> in which the product of external pressure by volume ( $PV$ ) is replaced by a function of the volume,  $\psi(V)$ , that conveys the information on the pressure. In this case one would have  $\nu(\mathbf{r}, V) \equiv V_{\text{ext}}(\mathbf{r}, V) + \psi(V)/N$ . Furthermore, taking into account that any definition of  $\delta_V$  can be addressed by  $\nu$ , without any loss of generality we shall consider a constant volume-scale, in spite of the recent controversy about the correct definition of  $\delta_V$ .<sup>7–12</sup>

The logarithm of  $\Delta_N$  is a functional of  $\nu$  and its derivative defines the generalized volume-dependent density  $n(\mathbf{r}, V)$ . From Eqs. (1) and (2) we obtain

$$n(\mathbf{r}, V) \equiv -k_B T \frac{\delta \log \Delta_N}{\delta \nu(\mathbf{r}, V)} = \omega(V) \rho_N(\mathbf{r}, V), \quad (3)$$

where  $\rho_N$  is the inhomogeneous density in the canonical ensemble and

$$\omega(V) = \frac{\mathcal{Q}_{N,V}[\nu]}{\int_0^\infty \mathcal{Q}_{N,V}[\nu] dV} = \frac{\mathcal{Q}_{N,V}[V_{\text{ext}}]}{\delta_V \Delta_N} e^{-\beta P V} \quad (4)$$

is the volume probability density. We note that the *usual* inhomogeneous density  $\rho$  can be written in the isothermal-isobaric ensemble as a volume average of canonical densities, i.e.,

$$\rho(\mathbf{r}) = \int_0^\infty \omega(V) \rho_N(\mathbf{r}, V) dV = \int_0^\infty n(\mathbf{r}, V) dV. \quad (5)$$

In order to obtain a *free-energy* functional  $\mathcal{F}$  of the density  $n(\mathbf{r}, V)$ , we perform the Legendre transform of  $-\log \Delta_N$ , i.e.,

$$\beta \mathcal{F}[n] = -\log \Delta_N[\nu[n]] - \beta \int n(\mathbf{r}, V) \nu(\mathbf{r}, V; [n]) d\mathbf{r} dV, \quad (6)$$

where we have made explicit that  $\nu$  is the potential that determines  $n$ . Given the structure of  $n$  as a product of  $\omega(V)$  times the canonical density  $\rho_N$  [see Eq. (3)] and the relation (2) between  $\Delta_N$  and the canonical partition function, from Eq. (6) one can obtain the following expression for the isothermal-isobaric functional  $\mathcal{F}$ :

$$\beta \mathcal{F}[n] = \int \omega(V) \log[\delta_V \omega(V)] dV + \int \omega(V) \beta \mathcal{F}_c[\rho_N] dV, \quad (7)$$

where  $\mathcal{F}_c[\rho_N]$  is the free-energy functional in the canonical ensemble, and, in terms of  $n$ , one has

$$\omega(V) = \frac{1}{N} \int n(\mathbf{r}, V) d\mathbf{r}, \quad (8)$$

and

$$\rho_N(\mathbf{r}, V) = \frac{N n(\mathbf{r}, V)}{\int n(\mathbf{r}, V) d\mathbf{r}}, \quad (9)$$

where the number of particles  $N$  is related to  $n(\mathbf{r}, V)$  through the constraint

$$\int n(\mathbf{r}, V) d\mathbf{r} dV = N. \quad (10)$$

Finally, the variational principle of density functional theory leads to the following Euler–Lagrange equation:

$$\frac{\delta \mathcal{F}[n]}{\delta n(\mathbf{r}, V)} + \nu(\mathbf{r}, V) = \lambda, \quad (11)$$

where  $\lambda$  is a Lagrange multiplier (independent of  $\mathbf{r}$  and  $V$ ) that accounts for the fixed- $N$  constraint (10). One can check (after tedious calculations) that this Euler–Lagrange equation together with the isothermal-isobaric functional (7) and Eqs. (8)–(10) yields the desired result for the density [Eq. (3)].

The free-energy functional of the ideal gas in the canonical ensemble is given by<sup>13,14</sup>  $\mathcal{F}_{c,\text{id}}[\rho_N] = \int \rho(\mathbf{r}) (\log(\Lambda^3 \rho(\mathbf{r}) - 1)) d\mathbf{r} + \phi(N)$ , where  $\Lambda$  is the thermal wavelength and  $\phi(N)$  is a function of the number of particles that, due to the constraint (10), does not affect the result of Eq. (11). Substituting this expression into Eq. (7) we obtain the following result for the *free-energy* functional of the ideal gas in the isothermal-isobaric ensemble:

$$\beta \mathcal{F}_{\text{id}}[n] = \frac{1-N}{N} \int n(\mathbf{r}, V) \log \left[ \delta_V \int n(\mathbf{r}, V) d\mathbf{r} \right] d\mathbf{r} dV + \int n(\mathbf{r}, V) \log[\delta_V \Lambda^3 n(\mathbf{r}, V)] d\mathbf{r} dV, \quad (12)$$

where an irrelevant function of  $N$  has been neglected. The excess (over-ideal) contribution to the isothermal-isobaric functional is directly obtained from Eqs. (7) and (12), one has

$$\mathcal{F}_{\text{ex}}[n] \equiv \mathcal{F}[n] - \mathcal{F}_{\text{id}}[n] = \frac{1}{N} \int n(\mathbf{r}, V) \mathcal{F}_{c,\text{ex}}[\rho_N] d\mathbf{r} dV, \quad (13)$$

where  $\mathcal{F}_{c,\text{ex}}$  is the excess contribution to the free energy in the canonical ensemble. An accurate expression for this excess quantity can be obtained by noting that the (total) free-energy functional in the canonical ensemble can be approximated by<sup>15</sup>

$$\mathcal{F}_c[\rho] \approx \mathcal{F}_{\text{gc}}[\rho] + \frac{1}{2} \log 2\pi \Delta^2(N; [\rho]), \quad (14)$$

where  $\mathcal{F}_{\text{gc}}[\rho]$  is the grand-canonical intrinsic free energy functional and  $\Delta^2(N; [\rho])$  is the mean square fluctuation of the number of particles. A given prescription for  $\mathcal{F}_{\text{gc}}$  is required. In the present work we have employed the customary fundamental measures theory (FMT) of Rosenfeld.<sup>16</sup>

From a practical viewpoint, to obtain an explicit expression for the density  $n(\mathbf{r}, V)$  one simply has to calculate the canonical profile  $\rho_N(\mathbf{r}, V)$  via

$$\rho_N(\mathbf{r}, V) = \Gamma(V) N \exp \left( -\beta \nu - \frac{\delta \beta \mathcal{F}_{c,\text{ex}}}{\delta \rho_N} \right), \quad (15)$$

where  $\Gamma(V)$  is a function that, fixed  $V$ , ensures proper normalization of  $\rho_N$ , i.e.,  $\Gamma(V) = 1/\int d\mathbf{r} \exp(-\beta \nu - \delta \beta \mathcal{F}_{c,\text{ex}}/\delta \rho_N)$ . Once  $\rho_N(\mathbf{r}, V)$  is known, the volume probability density is directly obtained from

$$\omega(V) = A \Gamma^N(V) \exp \left( -\beta \mathcal{F}_{c,\text{ex}} + \int d\mathbf{r} \frac{\delta \beta \mathcal{F}_{c,\text{ex}}}{\delta \rho_N} \rho_N \right), \quad (16)$$

where  $A$  is the normalization constant that grants  $\int_0^\infty \omega(V) dV = 1$ . Of course, this expression for  $\omega(V)$  is equal to Eq. (4) conveniently rewritten for our DFT calculation. We note that one can consider that while  $\rho_N$  carries the information on the microscopic structure of the fluid, the thermodynamic information is mainly addressed by  $\omega(V)$ .

### III. HARD SPHERES IN A SPHERICAL CAVITY

As an application of the present theoretical framework we have considered a fluid of hard spheres of diameter  $\sigma$  confined to a hard spherical cavity with fluctuating radius  $R_{\text{cav}}$ . In this case, the external potential is

$$V_{\text{ext}}(\mathbf{r}, R_{\text{cav}}) = \begin{cases} 0, & r < R_{\text{cav}} - \sigma/2 \\ \infty, & r > R_{\text{cav}} + \sigma/2, \end{cases} \quad (17)$$

which defines the volume available to the center of the hard spheres as  $V = 4\pi(R_{\text{cav}} - \sigma/2)^3/3$ . This expression for  $V$  can be trivially inverted so that the generalized potential becomes  $\nu(\mathbf{r}, V) = V_{\text{ext}}(\mathbf{r}, R_{\text{cav}}(V)) + PV/N$ . The accuracy of the theory has been tested against isothermal-isobaric Monte Carlo (MC) simulations. In our simulations we have considered  $(N+1) \times 10^8$  MC steps to equilibrate the system and the same number of steps to perform the measurements (every  $N+1$  steps). A MC step consists of selecting either a particle displacement or a volume change with probabilities  $N/(N+1)$  and  $1/(N+1)$ , respectively. To perform a volume change, a new value for the radius of the cavity  $R_{\text{new}}$  is randomly chosen in the interval  $[R_{\text{cav}} - r_{\text{max}}, R_{\text{cav}} + r_{\text{max}}]$ . The change is accepted with probability

$$p = \min \left\{ 1, \exp \left[ -\frac{4}{3} \pi \beta P \left( \left( R_{\text{cav}} - \frac{\sigma}{2} \right)^3 - \left( R_{\text{new}} - \frac{\sigma}{2} \right)^3 \right) + 2 \log \frac{R_{\text{cav}} - \frac{\sigma}{2}}{R_{\text{new}} - \frac{\sigma}{2}} \right] \right\}. \quad (18)$$

When the change implies a reduction on the radius of the cavity and the new cavity overlaps with any particle the change is rejected. The parameter  $r_{\text{max}}$  is chosen so that the overall acceptance ratio is about 30% of all attempts to perform a volume change. The same ratio is considered for the particle displacements. We note that we have not used scaled coordinates in the simulations.

When the theory is applied to systems at low pressures we obtain density profiles like those depicted in Fig. 1. In this case the mean density is very low and a quasi-ideal-gas profile is obtained. As expected for a low density situation, the figure shows excellent agreement between theory and simulation, both for the density profile,  $\rho(r)$ , and for the volume probability density,  $\omega(V)$ . We note that the present isothermal-isobaric profiles do not show the usual discontinuity at contact with the cavity hard-wall (see, e.g., Ref. 17). Of course, this is due to the weighted average of canonical density profiles for different cavity radii. This average gives rise to a smooth density profile at the border of the cavity. As  $N$  increases, the relative width of this *smooth* region decreases.

At higher pressures the agreement between theory and simulation is still very good except for some situations in which the density profile develops a pronounced peak in the center of the cavity. This is the situation presented in Fig.

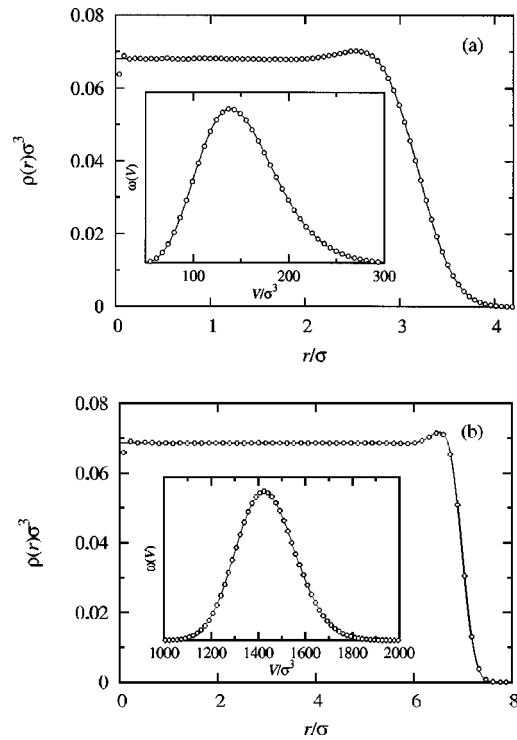


FIG. 1. Isothermal-isobaric density profiles of hard spheres in a spherical cavity [see Eq. (5)].  $\beta P = 0.08\sigma^{-3}$  and (a)  $N = 10$ , (b)  $N = 100$ . Solid lines, DFT results; circles, simulation results. The insets show the volume probability density  $\omega(V)$ .

2(a), where both the simulation and the DFT results for the density profile of  $N = 10$  particles exhibit this peak but it is clear that the theory cannot describe it accurately. This problem also arises for similar situations in other ensembles<sup>15,17-19</sup> and will be studied in more detail in the following section. Things are different in Fig. 2(b) ( $N = 100$ ) where the central peak is absent and the agreement with simulation is excellent.

If we now pay our attention to the volume probability densities (see the insets of Fig. 2) we observe that the theory and simulation results for  $\omega(V)$  are slightly shifted with respect to each other. This can be ascribed to small deviations in the calculation of the free energy at high packings—note that in the homogeneous limit the FMT yields the Percus–Yevick equation of state<sup>16</sup>—and hence of the volume probability density. The shift in  $\omega(V)$  gives rise for theory and simulation to different mean volumes,  $\langle V \rangle \equiv \int_0^\infty V \omega(V) dV$ . For instance, when  $N = 100$  and  $\beta P = 3.2\sigma^{-3}$ ,  $\langle V \rangle = 122.498\sigma^3$  for the DFT and  $\langle V \rangle = 122.015\sigma^3$  for the MC simulation.

A way to avoid the shift in  $\omega(V)$  is to compare results with the same mean volume rather than with the same pressure. In essence, this is the procedure applied in Ref. 17, where equal mean number of particles (instead of equal chemical potential) was imposed when comparing canonical and grand-canonical results. When this scheme is applied to the situation of Fig. 2(b) ( $N = 100$  and  $\beta P = 3.2\sigma^{-3}$ ) one finds that the DFT profile must be calculated at a pressure of  $\beta P = 3.22932\sigma^{-3}$  in order to obtain the mean volume of the MC simulation. This implies a difference in the pressure of

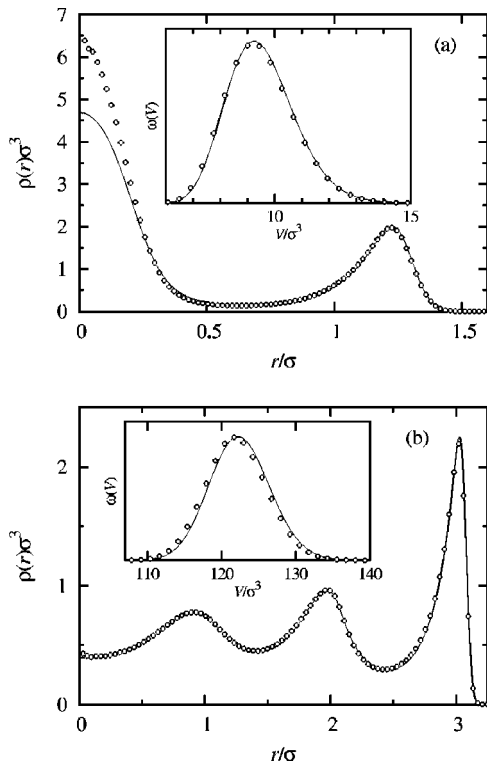


FIG. 2. Same as in Fig. 1 but for  $\beta P = 3.2\sigma^{-3}$ .

about 0.92%. As one can observe in Fig. 3, this procedure only appreciably improves the results for the volume probability density while the profile remains almost unchanged. It is clear that the effect of the mean-volume shift is washed out by the structure of the density profile.

#### IV. ANALYSIS OF THE DENSITY PROFILE IN THE CENTER OF THE CAVITY

In the preceding section we have seen [Fig. 2(a)] that the density profile of  $N=10$  particles at pressure  $\beta P = 3.2\sigma^{-3}$  presents a pronounced peak in the center of the cavity whereas this peak is missing for  $N=100$  at the same external pressure. It seems therefore natural to analyze the behavior of the peak for different numbers of particles in order to ascertain the influence of  $N$  in the structure of the confined fluid. Furthermore, since the main differences between

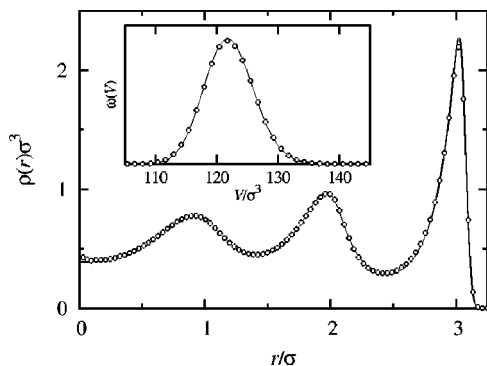


FIG. 3. Same as in Fig. 2(b) but for equal mean volume. MC pressure,  $\beta P = 3.2\sigma^{-3}$ . DFT pressure  $\beta P = 3.22932\sigma^{-3}$ .  $N=100$ .

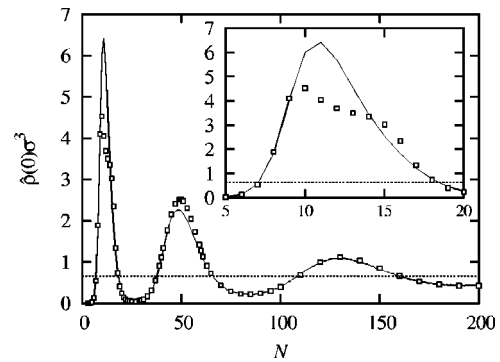


FIG. 4. Mean density in the center of the cavity as a function of the number of particles (see text). For clarity, the solid lines are simulation results and the symbols ( $\square$ ) are DFT results. The inset shows an enlarged view of the first peak.  $\beta P = 3.2\sigma^{-3}$ . The dashed line indicates the bulk density.

theory and simulation arise in this peak, we expect to obtain information about the reasons for the failure of the DFT in this situation. We note that, in contrast to previous approaches for this quasi-zero-dimensional problem,<sup>15,17,18</sup> the volume of the system changes in order to accommodate the different numbers of particles according to the fixed external pressure. Thus, the present ensemble with fluctuating volume provides a good framework for the analysis of the behavior of the peak with  $N$ .

Figure 4 shows the results of theory and simulation for the density  $\rho$  in the center of the cavity, for  $N$  ranging between 2 and 200 at  $\beta P = 3.2\sigma^{-3}$ . We have estimated the value of  $\rho(0)$  in simulation by measuring the mean density,  $\hat{\rho}(0)$ , in a small sphere of radius  $r_0$  situated at the center of the cavity. We have taken  $r_0 = 0.076\sigma$  that yields rather smooth simulation results. For the sake of consistency, we have considered  $\hat{\rho}(0) = \int_0^{r_0} \rho(r) 4\pi r^2 dr / (\frac{4}{3}\pi r_0^3)$  for the DFT results. Also, we have plotted the value of the bulk density,  $\rho_b = 0.65\sigma^{-3}$ , that, via the Carnahan–Starling equation of state, corresponds to the pressure of the system.

The most relevant feature of Fig. 4 is the appearance of a well defined peak structure so that for certain values of  $N$  there is a large probability of finding a particle in the center of the cavity, whereas for other values this probability becomes very close to zero. As expected, for large  $N$  the mean density  $\hat{\rho}(0)$  approaches the bulk density  $\rho_b$ . It is important to remark that the three maxima of  $\hat{\rho}(0)$  in the simulation data are attained at  $N=11, 49$ , and  $129$ , very close to the numbers ( $N=13, 55$ , and  $147$ ) that arise when spheres are packed closely together in concentric layers around a central sphere. Of course we are far away from close packing but it is nevertheless interesting to see how the development of a central peak in the profile is related to these *magic* numbers.

As mentioned previously, the peaks in Fig. 4 correspond to the larger differences between simulation and DFT results. This is specially noticeable in the first peak (see the inset) where we note that while the theory is accurate for  $N \leq 9$ , it clearly underestimates the value of the density in the center of the cavity for  $10 \leq N \leq 13$  and slightly overestimates it for larger values of  $N$ . A different behavior is found in the second peak where the results of simulation lie below those of DFT. In the third peak the differences between theory and

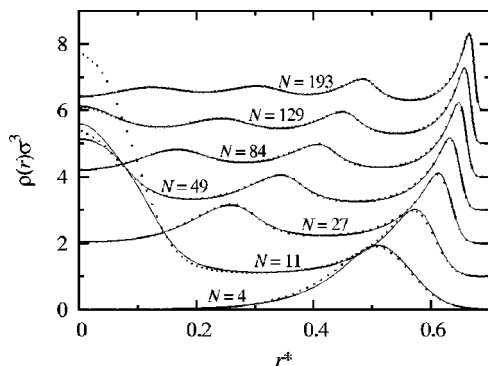


FIG. 5. Isothermal-isobaric density profiles at  $\beta P = 3.2\sigma^{-3}$  for different values of  $N$ . The lines are the results of the theory and the symbols ( $\circ$ ) are simulation data. The profiles have been shifted vertically and the radius has been rescaled in terms of  $N$  [ $r^* \equiv r/(\sigma N^{1/3})$ ].

simulation are very small but larger than in the neighboring regions. It seems therefore that the discrepancies found are mainly due to the large inhomogeneity in the density profile although, in our opinion, the occurrence of a quasi-zero-dimensional situation also plays an important role, possibly due to the fact that the large fluctuations expected for this zone are not accurately described by the present (mean field) DFT theory.<sup>15,17,18</sup>

Figure 4 shows the manner in which the layer structure is originated with  $N$  increasing, once the external pressure is fixed. For  $N < 7$  there is only one external layer and the mean density in the center of the cavity is very small, see, e.g., the case  $N = 4$  in Fig. 5. For  $N \geq 7$  a peak develops in the center of the cavity, attaining its maximum value for  $N = 11$ . This profile is plotted in Fig. 5, where we can see the failure of the theory in the central zone. For  $N > 11$  the height of the peak starts to decrease and a second layer steadily appears. This layer is clearly apparent in the range  $19 < N < 39$  where the density is very small in the center of the cavity (see the case  $N = 27$  in Fig. 5). Again, for  $N > 40$  the central peak grows, reaching its maximum at  $N = 49$ , now with a value much smaller than that of the peak near  $N = 11$  but comparable to the height of the density profile near the cavity wall. This scheme is repeated for the following peak but now the amplitude of oscillation about the bulk is very small and one can hardly speak of a quasi-zero-dimensional situation (see  $N = 129$  in Fig. 5). We note that, except for the maxima of the two main peaks,  $N = 11$  and  $N = 49$ , the overall performance of the theory is very good.

At higher pressures the system becomes very inhomogeneous and the DFT approach fails, specially for values of  $N$  close to the location of the peaks of Fig. 4. A simulation analysis shows that increasing the pressure yields the same behavior for the mean density in the center of the cavity but with much higher peaks, with almost unchanged location. For certain values of  $N$ , below the maxima of the peaks, we have observed that as the pressure increases the mean density in the center grows until it reaches a maximum and then it gradually decreases to zero. It seems that the packing constraints in the problem give rise to a change in the structure of the confined fluid from a situation with large mean density in the center to a situation with very small mean density. This

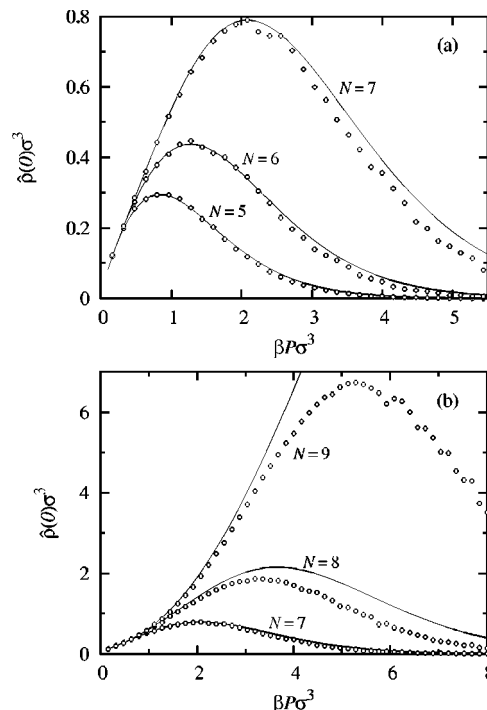


FIG. 6. Mean density in the center of the cavity as a function of the pressure. The lines are simulation results and the symbols are DFT results. (a)  $N = 5, 6$ , and  $7$ ; (b)  $N = 7, 8$ , and  $9$ . For comparison, the case  $N = 7$  is plotted in both panels. Note the different scales.

noticeable behavior is depicted in Fig. 6 for  $N$  ranging between 5 and 9. Finally, we observe that the agreement between theory and simulation is very good for  $N \leq 7$  [Fig. 6(a)], much worse for  $N = 8$ , and very bad for  $N = 9$  [Fig. 6(b)]. In the latter case the DFT results grossly overestimate the simulation results for  $\beta P \geq 4\sigma^{-3}$ . We have observed the same behavior for values of  $N$  below the second peak in Fig. 4.

## V. SUMMARY

In summary, we have presented a new DFT method for dealing with inhomogeneous fluids in the isothermal-isobaric ensemble. We have shown that rewriting the isothermal-isobaric partition function as a functional of the generalized external potential  $\nu(\mathbf{r}, V)$  allows one to introduce the volume-dependent density  $n(\mathbf{r}, V)$ , in terms of which the theory is formulated. The method is very general since  $\nu(\mathbf{r}, V)$  contains all the information concerning the external pressure and the volume-scale of the ensemble and, consequently, the theory is transparent to any particular choice of volume-scale or fluctuating volume ensemble. The main result of this paper is a very simple, exact expression for the isothermal-isobaric *free-energy* functional. The only input required by this expression is the free-energy functional in the canonical ensemble.

As an application we have considered a hard-sphere fluid confined to a spherical cavity with fluctuating radius. In general, the theory yields very good results when compared with our MC simulations of the system. In some situations, however, we have found that the density profile of the fluid develops a pronounced peak in the center of the cavity that the

DFT theory cannot reproduce accurately. The appearance of this peak is strongly related to the number of particles in the cavity, reaching its maximum influence for values of  $N$  close to the *magic* numbers 13, 55, and 147. In general, as expected, the peak grows as the pressure of the system is increased. However, for certain numbers of particles (see Fig. 6), we have observed that when the pressure reaches a given value the growth of the peak is stopped and a further increase of the pressure leads to the vanishing of the peak. This behavior indicates a transition in the structure of the system from a situation with strong localization in the center of the cavity to a situation where the mean density in this zone is very low.

#### ACKNOWLEDGMENTS

J.A.W. thanks J. A. Cuesta for suggesting the formulation of DFT in the isothermal-isobaric ensemble. We thank financial support by the Ministerio de Ciencia y Tecnología of Spain under Grant Nos. BFM2002-01225 FEDER and BFM2003-07106 FEDER, and by Junta de Castilla y León y F.S.E. under Grant No. SA092/04.

- <sup>1</sup>J. P. Hansen and I. R. McDonald, *Theory of Simple Liquids* (Academic, London, 1991).
- <sup>2</sup>D. Frenkel and B. Smit, *Understanding Molecular Simulation* (Academic, London, 1996).
- <sup>3</sup>D. Ruelle, *Statistical Mechanics: Rigorous Results* (Benjamin, New York, 1969).
- <sup>4</sup>C. Tutschka and J. A. Cuesta, *J. Stat. Phys.* **111**, 1125 (2003).
- <sup>5</sup>J. K. Percus, *J. Stat. Phys.* **100**, 2417 (2002).
- <sup>6</sup>P. Attard and G. A. Moule, *Mol. Phys.* **78**, 943 (1993).
- <sup>7</sup>P. Attard, *J. Chem. Phys.* **103**, 9884 (1995).
- <sup>8</sup>G. J. M. Koper and H. Reiss, *J. Phys. Chem.* **100**, 422 (1996).
- <sup>9</sup>D. S. Corti and G. Soto-Campos, *J. Chem. Phys.* **108**, 7959 (1998).
- <sup>10</sup>D. S. Corti, *Phys. Rev. E* **64**, 016128 (2001).
- <sup>11</sup>K.-K. Han and H. S. Son, *J. Chem. Phys.* **115**, 7793 (2001).
- <sup>12</sup>D. S. Corti, *Mol. Phys.* **100**, 1887 (2002).
- <sup>13</sup>J. A. White and S. Velasco, *Europhys. Lett.* **54**, 475 (2001).
- <sup>14</sup>J. A. White and A. González, *J. Phys.: Condens. Matter* **14**, 11907 (2002).
- <sup>15</sup>J. A. White, A. González, F. L. Román, and S. Velasco, *Phys. Rev. Lett.* **84**, 1220 (2000).
- <sup>16</sup>Y. Rosenfeld, *Phys. Rev. Lett.* **63**, 980 (1989).
- <sup>17</sup>A. González, J. A. White, F. L. Román, and R. Evans, *J. Chem. Phys.* **109**, 3637 (1998).
- <sup>18</sup>A. González, J. A. White, F. L. Román, S. Velasco, and R. Evans, *Phys. Rev. Lett.* **79**, 2466 (1997).
- <sup>19</sup>Z. T. Németh and H. Löwen, *J. Phys.: Condens. Matter* **10**, 6189 (1998).